Ice-albedo feedback in the Northern Hemisphere during the Last Glacial Maximum

Melissa A. Burt
Department of Atmospheric Science
Colorado State University
Fort Collins, CO

David A. Randall
Department of Atmospheric Science
Colorado State University
Fort Collins, CO

Bette L. Otto-Bliesner
Climate and Global Dynamics Division
National Center for Atmospheric Research
Boulder, CO

_____

Corresponding author: Melissa A. Burt, Department of Atmospheric Science, Colorado State

University, 1371 Campus Delivery, Fort Collins, CO 80523.

Tel: (970) 491-8706, Fax: (970) 491-8693, email: mburt@atmos.colostate.edu

Abstract

We use simulations performed with the Community Climate System Model version 3 (CCSM3), a coupled global climate model, to examine the role of the ice-albedo feedback in the Northern Hemisphere for the Last Glacial Maximum (LGM) and Pre-Industrial (PI) climates. The simulated PI climate is 4.9 Celsius warmer globally than the LGM climate, with the greatest warming in the high latitudes of both hemispheres. The positive ice-albedo feedback acts to amplify the climate change as a consequence of the melting of sea ice and ice sheets in the Northern Hemisphere. An unexpected and interesting result is that the ice-albedo feedback is negative in some regions, particularly in the Arctic Ocean, because of an increased ocean basin size at PI. We investigate the roles of ocean basin size, snow cover, sea ice, and incoming solar radiation in determining this result.

Index Terms: 3344 Paleoclimatology; 3337 Global climate models; 4908 Albedo; 3305 Climate change and variability; 1621 Cryospheric change; 1635 Oceans; 1641 Sea level change

1. **Introduction**

      The Last Glacial Maximum (LGM), which occurred approximately 21 ka (21,000 years ago), was the peak of the last glacial period, when large inland ice sheets reached their maximum volume in the Northern Hemisphere. The combined effects of the ice sheets and sea ice had a major impact on the radiation budget of the Earth. In this paper, we focus on the ice-albedo feedback during the transition from the Last Glacial Maximum to Pre-industrial (PI, i.e., the period before industrialization, nominally at 1800 A.D) [*Otto-Bliesner et al., 2006*].

      The albedos of the open ocean and sea ice are approximately 0.06 and 0.6, respectively. Because of this, sea ice area has a strong role in the ice-albedo feedback [*Bony et al., 2007*]. If snow is present on the surface of the sea ice, it acts as an insulator, increases the albedo, and further reduces the temperature. As a result, melting is reduced or delayed. As the climate warms, sea ice melts, the highly reflective surface is replaced by a much less reflective one, and the amount of solar radiation absorbed at the surface increases. This enhances the initial warming caused by the external perturbation, resulting in a positive feedback. Changes in sea ice extent and thickness affect the sensible and latent heat fluxes, and result in a redistribution of heat in the system [*Hall, 2004*]. This results in a maximum of polar warming during the winter and fall months, when the atmosphere responds to reduced sea ice thickness, increased turbulent fluxes, and more open ocean water due to increased solar absorption during the preceding summer months [*Bony et al., 2007*].

      Here we present an analysis of results from the Paleoclimate Modeling Intercomparison Project (PMIP-2), focusing on simulations performed with the Community Climate System Model Version 3 (CCSM3), developed at the National Center for Atmospheric Research

(NCAR). We focus on the role of the ice-albedo feedback during the transition from the Last

Glacial Maximum to Pre-Industrial climate and the mechanisms behind this feedback.

2. **Model description and forcings**

Simulations were conducted with the Community Climate System Model Version 3. CCSM3 includes representations of the atmosphere, ocean, sea ice, and land surface. A full description of the model is given by *Collins et al.* [*2006*]. Briefly, the atmosphere model uses the primitive equations, with a resolution of T42, corresponding to a grid with 128 by 64 cells (approximately 2.8º grid spacing). The land-surface model uses the same grid as the atmosphere model. The ocean model has a grid of 320 x 384 points; the poles of the "stretched" grid are located in Greenland and Antarctica. The grid spacing of the ocean model is nominally 1º by 1º latitude and longitude, with greater resolution in the Tropics and North Atlantic. The dynamic-thermodynamic sea ice model is implemented on the ocean model's horizontal grid, and uses the elastic-viscous-plastic rheology to simulate sub-grid scale ice thickness, and the movement of the sea ice pack as driven by ocean currents [*Hunke and Dukowicz, 1997*]. The component models are linked using a coupler through which fluxes and state information are exchanged. Coupling and spin-up procedures for the simulations are described by *Otto-Bliesner et al.* [*2006*].

The LGM simulation uses specified continental ice cover and elevation taken from the ICE-5G (VM2) ice sheet reconstruction, in which massive ice sheets cover North America, Europe, Greenland, and Antarctica [*Peltier, 2004*]. Sea level is lowered by approximately 120 meters relative to the present day, using the ETOPO topography-bathymetry dataset and adjusting the land mask to match *Peltier [2004]* [*Otto-Bliesner et al., 2006*]. As a result, land is exposed, including the land bridge between Asia and Alaska, portions of the Indonesian Archipelago between Australia and New Guinea, and a region stretching from France and the British Isles to Svalbard and the arctic coastline of Eurasia [*Otto-Bliesner et al., 2006*]. The mechanisms behind this sea level change are: 1) thermal expansion; 2) the exchange of water

between oceans and other reservoirs (e.g. glaciers, ice sheets, etc.); and 3) global isostatic adjustment, which occurs in response to changes in external surface loads, particularly during glaciation and deglaciation *[Peltier, 2004]*.

Figure 1 is a North Polar stereographic map of the land and ocean at LGM and PI. Regions that are land for both LGM and PI are shown in grey, and "additional" land at LGM, due to lowered sea level, is shown in black. The Arctic Ocean basin size (north of 66° N) was 7.98 million km^2 at LGM and 13.09 million km^2 at PI (see Table 1). The Arctic Ocean was thus significantly larger at PI, due to the rise in sea level.

Atmospheric aerosols and the solar constant were set at their Pre-industrial values for both simulations. LGM atmospheric trace gases were inferred from ice core measurements (CO_2 = 185 ppmv, CH_4= 350 ppbv, and N_2O = 200 ppbv). The key forcings and boundary conditions for the LGM simulation are the large ice sheets, atmospheric trace gases, aerosols, sea level, and vegetation, in addition to the relatively weak Milankovitch orbital forcings [*Otto-Bliesner et al., 2006*]. Forcings for the Pre-industrial simulation correspond to approximately 1800 AD. Concentrations of PI atmospheric trace gases were fixed at CO_2 = 280 ppmv, CH_4= 760 ppbv, and N_2O = 270 ppbv, as inferred from ice core measurements. The reduced concentrations of LGM atmospheric trace gases, relative to PI, result in a total decrease in radiative forcing of the troposphere 2.76 W m^{-2}. The majority of the change results from a decrease of CO_2 [*Otto-Bliesner et al., 2006*]. PMIP-2 simulations neglect changes in dust and vegetation, which could potentially have large impacts regionally in the LGM simulation. It has been estimated that if dust were incorporated the resulting global forcing would be -1 W m^{-2} [*Braconnot et al., 2007*].

3. Results

　　We compare averages based on the last 100 years of the LGM and PI simulations. During the transition from the glacial to interglacial climate, some of the most significant changes were in the global mean temperature, sea level, and the extent and area of sea ice. Changes in the sizes of the ocean basins affect the sea ice area, and thus also affect the surface albedo.

3.1 **Northern Hemisphere Sea Ice**

　　As expected, the globally averaged sea ice area decreased from LGM to PI. The simulated Northern Hemisphere sea ice area, sea ice thickness, and snow thickness are shown in Figure 2. The simulated annual Northern Hemisphere sea ice area at LGM was 11.61 million km^2 and increased to 13.35 million km^2 at PI. The annual Northern Hemisphere sea ice area was computed by averaging the amount of ice area in the extratropics (20º-90º N). During the transition between LGM and PI, there is a significant decrease in the amount of sea ice in the Southern Hemisphere (not shown), but interestingly there is an increase in the Northern Hemisphere sea ice at PI, due to the larger Arctic Ocean basin (Figure 2). The Arctic Ocean is completely ice covered, in both simulated climates. At LGM, extensive sea ice extends eastward into the North Atlantic and North Pacific Oceans and equatorward, down to 50º N annually and 45º N in winter. This favors a southward shift of the Gulf Stream and storm tracks, in the Atlantic and Pacific Oceans. *Otto-Bliesner et al.* [*2006*] found that CCSM3 overestimates the winter extent of sea ice at LGM compared to foraminifera paleotemperature estimates made by *Sarnthein et al.* [*2003*] for the North Atlantic. At PI, the eastward and equatorward extents of sea ice in the Atlantic and Pacific basins have decreased dramatically.

During winter, the simulated sea ice thickness is considerably greater at LGM than at PI. Sea ice thicknesses are 6-7 meters over the Arctic and Greenland regions at LGM and several meters thinner at PI. Sea surface temperatures are 0.5 K warmer in this region at PI, which can be both a cause and effect of the thinning ice.

It is difficult to assess the realism of the sea ice distribution at PI, simulated by CCSM3, since there is a lack of "good" data. Significantly more observational data are available at Present-day, and therefore can be used to evaluate how well the model captures the distribution of sea ice. Present-day climate simulations by *Holland et al. [2006]* concluded that CCSM3 sea ice distributions are "quite good" and "reasonably capture" the sea ice concentration, despite a few biases, compared to observations taken from Special Sensor Microwave Imager (SSM/I) data.

The presence of snow cover on the sea ice has a significant impact on the area-averaged surface albedo. In the model, there is a direct relationship between snow cover and surface albedo, as snow cover increases, surface albedo increases. As shown in Figure 2, there is up to 0.5 meters of simulated snow cover (depth) on the surface of the sea ice in the Arctic Ocean at LGM. The amount of simulated snow cover decreases near the land-ocean boundaries. At PI, snow cover on the ice surface has diminished in the center of the Arctic Ocean, but has increased near the coast. Snowfall rates on land (not shown), have decreased globally between PI and LGM, except for Greenland, where snowfall increases by up to 0.3 mm day^{-1} during the summer months. Increased snowfall on Greenland is due to increased transport of moisture by eddies into the region.

3.2 **Ice-albedo feedback**

We quantified the ice-albedo feedback in a simplified manner, analyzing the globally

averaged clear-sky reflected shortwave radiation at the surface for each simulation. The clear-sky reflected shortwave radiation was determined by subtracting the clear-sky net solar flux at the surface from the clear-sky downwelling shortwave radiation at the surface. Table 2 gives the ice-albedo feedback for LGM, PI, and PI minus LGM, and also shows the feedback strength, defined as the change in energy flux divided by the change in temperature. As expected, the *global* ice-albedo feedback is positive from LGM to PI; the change in the clear-sky absorbed shortwave at the surface is 11.68 W m^{-2} giving a climate change feedback strength of 2.38 W m^{-2} K^{-1} (based on the simulated surface temperature change of 4.9 K).

For the Northern Hemisphere, the result is different. Table 3 shows the annual and seasonal Northern Hemisphere all-sky and clear-sky reflected shortwave radiation at the surface (ocean only), in both W m^{-2} and Watts, for LGM, PI, and PI minus LGM. Results are also shown for the Southern Hemisphere, for comparison. From LGM to PI, there are decreases in the all-sky and clear-sky reflected shortwave at the surface during each season, except during the summer months, when the clear-sky reflected shortwave radiation *increases* by 0.11 W m^{-2}. The JJA increase in clear-sky reflected shortwave radiation is related to the greater top-of-atmosphere insolation received at PI *[Otto-Bliesner et al. 2006, Figure 1]*. This is also seen during DJF in the Southern Hemisphere. There is a 14% increase in Arctic Ocean basin size at PI, allowing for less absorbed shortwave radiation by the ice; *the change in ocean basin size results in a negative ice-albedo feedback for this region*.

This can also be seen in Figure 3, which shows the JJA zonal mean clear-sky reflected shortwave radiation at the surface. The top panels show all land and ocean areas and the bottom panels are for the ocean only. The greatest changes in the clear-sky reflected shortwave at the surface are found in the high latitudes of both hemispheres. An exception occurs between the

North Pole and 60º N, where the clear-sky reflected shortwave radiation is greater at PI. In the all-sky cases (i.e., with cloud effects), more shortwave radiation is reflected at LGM.

Snow cover over both the land and ocean affect the surface albedo, and allows for more reflection and less absorption of solar radiation, resulting in an Arctic mean of 113 W m^{-2} for the clear-sky reflected shortwave radiation at LGM (not shown). A strong correlation exists between solar radiation absorbed or reflected by the surface and the thickness of the ice. *Ebert et al.,* [*1995*] found that the absorption of solar energy is a function of ice thickness. As ice thickness increases, the absorption coefficient decreases, mainly due to a decrease in air bubbles within the ice. The presence of snow cover also acts to enhance reflected solar radiation by the ice surface. Clear-sky shortwave radiation reflected by the surface is dramatically reduced, by roughly 50%, at PI, due to the melting of land ice. Over the Arctic Ocean and Greenland, the solar energy reflected increases by 50 W m^{-2} from LGM to PI. This occurs as a result of increased summer solar insolation and more snowfall over land and ice in these regions, in correspondence with the difference plot shown in Figure 4. There are some places on the land-ocean boundary, where the reflected shortwave radiation increases, due to the expansion of the Arctic Ocean and the presence of more sea ice, this is shown in red. We also found that in the regions where the surface albedo increased from LGM to PI, the warming from LGM to PI was less than in other regions at the same latitude. Between 70-73 degrees latitude, JJA surface temperature change from LGM to PI varied by 2.5 K.

4. **Conclusions**

We have analyzed the role of the ice-albedo feedback from the transition between the Last Glacial Maximum and Pre-Industrial. Although the positive ice-albedo feedback acts to amplify the climate change by 2.38 W m^{-2} K^{-1}, due to the melting of sea ice and ice sheets in the Northern Hemisphere, the ice-albedo feedback is actually negative over large regions of the high-latitude Northern Hemisphere, due to changes in the size of the Arctic Ocean basin.

Would the result of a negative ice-albedo feedback occur in the other PMIP-2 models? All of the PMIP-2 LGM simulations used the land-sea mask of *[Peltier 2004]*, interpolated to their specific resolutions, except for the MIROC model. Because of the difficulty in changing their ocean model grid, a hybrid of the land-sea mask was adapted, and incorporated the LGM land-sea mask in the atmosphere model but used present-day for the ocean model.

For future climate change simulations, would the same result occur when analyzing Present-day and the Future? Due to changes in sea level, we can assume that the Arctic basin will be larger, but warmer surface temperatures will result in little to no sea ice present. How will this affect the ice-albedo feedback in this region? *Bitz et al. [2006]* analyzed ocean heat uptake and sea ice sensitivity as a response to increasing CO_2 and determined that as CO_2 surpassed a level beyond doubling, during winter, sea ice growth will diminish, the Arctic overturning circulation will decrease, and as a result there will be a decline in northward heat transport into the Arctic. This will have a dramatic impact on the ice-albedo feedback in this region.

References

Bitz, C.M., P.R. Gent, R.A. Woodgate, M.M. Holland, and R. Lindsay (2006), The influence of sea ice on ocean heat uptake in response to increasing CO_2, *J. Climate*, **19**, 2437-2450.

Bony, S., R. Colman, V.M. Kattsov, R.P. Allan, C.S. Bretherton, J.-L. Dufresne, A. Hall, S. Hallegatte, M.M. Holland, W. Ingram, D.A. Randall, D.J. Soden, G. Tselioudis, and M.J. Webb (2006), How well do we understand and evaluate climate change feedback processes?, *J. Climate*, **19**, 3445-3482.

Braconnot, P., Otto-Bliesner, B., Harrison, S., Joussaume, S, Peterchmitt, J.-Y., Abe-Ouchi, A., Crucifix, M. , Driesschaert, E., Fichefet, Th., Hewitt, C. D., Kageyama, M., Kitoh, A., Laine, A., Loutre, M.-F., Marti, O., Merkel, U., Ramstein, G., Valdes, P., Weber, L. ,Yu, Y., and Zhao, Y. (2007), Results of PMIP2 coupled simulations of the mid-Holocene and Last Glacial Maximum - Part 1: experiments and large-scale features, *Clim. Past,* **3**, 261-277.

Collins, W.D., C.M. Bitz, M.L. Blackmon, G.B. Bonan, C.S. Bretherton, J.A. Carton, P. Chang, S.C. Doney, J.J. Hack, T.B. Henderson, J.T. Kiehl, W.G. Large, D.S. McKenna, B.D. Santer, and R.D. Smith (2006), The community climate system model version 3 (CCSM3*), J. Climate*, **19**, 2122-2143.

Ebert, E.E., J.L. Schramm, and J.A. Curry (1995), Disposition of solar radiation in sea ice and the upper ocean, *J. Geophys. Res*., **100**, 15,965-15,975.

Hall, A. (2004), The role of surface albedo feedback in climate. *J. Climate*, 17, 1550-1568.

Holland, M.M., C.M. Bitz, E.C. Hunke, W.H. Lipscomb, and J.L. Schramm (2006), Influence of the sea ice distribution on polar climate in CCSM3, *J. Clim.*, **19**, 2398-2414.

Hunke, E. C. and J. K. Dukowicz (1997), An elastic-viscous-plastic model for sea ice dynamics, *J. Phys. Oceanogr.*, **27**, 1849-1868.

Otto-Bliesner, B.L., E. Brady, G. Clauzet, R. Tomas, S. Levis, and Z. Kothavala (2006), Last glacial maximum and Holocene climate in CCSM3, *J. Climate*, **19**, 2526-2544.

Peltier, W.R. (2004), Global glacial isostasy and the surface of the ice-age Earth: the ICE-5G (VM2) model and GRACE, *Annu. Rev. of Earth and Planet. Sci.*, **32**, 111-149.

Sarnthein, M., U. Pflaumann, and M. Weinelt (2003), Past extent of sea ice in the northern North Atlantic inferred from foraminiferal paleotemperature estimates, *Paleoceaongraphy*, **18**(2), 1047, doi:10.1029/2002PA000771.

Table Captions

Table 1: Quantifying the ice-albedo feedback for the LGM, PI, and PI minus LGM in W m^{-2}. Feedback strength is shown in the far right column.

Table 2: Quantifying the ice-albedo feedback for the LGM, PI, and PI minus LGM in W m^{-2}. Feedback strength is shown in the far right column, based on a temperature change of 4.9 K.

Table 3: Northern Hemisphere all-sky and clear-sky reflected shortwave radiation at the surface (ocean only) for LGM, PI, and PI minus LGM in W m^{-2} (top) and Watts (bottom). The reflected shortwave radiation is shown in Watts to include changes in ocean basin size. Table 3 is separated into Annual, June-July-August (JJA), and December-January-February (DJF).

Figure Captions

Figure 1: North Polar stereographic map of land and ocean at Last Glacial Maximum and Pre-Industrial. Grey regions are land for both LGM and PI, and "additional" land at LGM, due to lowered sea level, is black .

Figure 2: Northern Hemisphere sea ice area in percent (left), sea ice thickness in meters (middle), and snow thickness (right) simulated by the CCSM3 for the LGM (top) and PI (bottom). The month of March was selected because it is the month of maximum sea ice cover in the Northern Hemisphere.

Figure 3: June-July-August (JJA) clear-sky zonally averaged reflected shortwave radiation in W m^{-2} at the surface for all areas (top) and the ocean only (bottom). Pre-Industrial is shown in black and the Last Glacial Maximum in red.

Figure 4: June-July-August (JJA) clear-sky surface albedo (top) in Wm^{-2} for PI minus LGM. No attempt has been made to reconstruct the continental outlines. Figure 1 is shown for comparison in the bottom panel.

Tables

Table 1. Surface area basin size for all oceans and the Arctic Ocean.

	Surface Area (km^2)	
	All Oceans	Arctic Ocean
LGM	344,307,800	7,979,200
PI	361,134,000	13,089,300
PI - LGM	16,826,200	5,110,100

Table 2: Quantifying the global ice-albedo feedback for the LGM, PI, and PI minus LGM in W m^{-2}. Feedback strength is shown in the far right column, based on a temperature change of 4.9 K.

	LGM	PI	PI-LGM	Feedback Strength
	W m^{-2}	W m^{-2}	W m^{-2}	W m^{-2} K^{-1}
Ice-Albedo				
Clear-sky reflected SW at surface	- 44.14	- 32.46	11.68	2.38

Table 3: Northern Hemisphere all-sky and clear-sky reflected shortwave radiation at the surface (ocean only) for LGM, PI, and PI minus LGM in W m^{-2} (top) and Watts (bottom). The reflected shortwave radiation is shown in Watts to include changes in ocean basin size. Table 3 is separated into Annual, June-July-August (JJA), and December-January-February (DJF).

Reflected Shortwave Radiation at the Surface (W m^{-2})

	Northern Hemiphere			Southern Hemiphere		
	LGM	PI	PI - LGM	LGM	PI	PI - LGM
Annual						
All-sky	10.26	9.99	-0.27	10.42	10.12	-0.30
Clear-sky	13.20	13.13	-0.07	13.47	13.45	-0.02
JJA						
All-sky	10.53	10.30	-0.23	9.03	8.43	-0.60
Clear-sky	13.39	13.50	0.11	12.24	11.85	-0.39
DJF						
All-sky	9.59	9.23	-0.36	11.73	11.60	-0.13
Clear-sky	12.94	12.67	-0.27	14.78	15.01	0.23

Reflected Shortwave Radiation at the Surface (Watts)

	Northern Hemiphere			Southern Hemiphere		
	LGM	PI	PI - LGM	LGM	PI	PI - LGM
Annual						
All-sky	9.16 E+14	1.00 E+15	8.40 E+13	1.22 E+15	1.39 E+15	-1.70 E+14
Clear-sky	1.18 E+15	1.32 E+15	1.40 E+14	1.57 E+15	1.85 E+15	-2.80 E+14
JJA						
All-sky	9.50 E+14	1.06 E+15	1.10 E+14	1.07 E+15	1.19E+15	-1.20 E+14
Clear-sky	1.21 E+15	1.38 E+15	1.70 E+14	1.45E+15	1.67E+15	-2.20 E+14
DJF						
All-sky	8.86 E+14	9.54 E+14	6.80 E+13	1.39 E+15	1.61 E+15	-2.20 E+14
Clear-sky	1.19 E+15	1.31 E+15	1.20 E+14	1.75E+15	2.08 E+15	-3.30 E+14

Figures
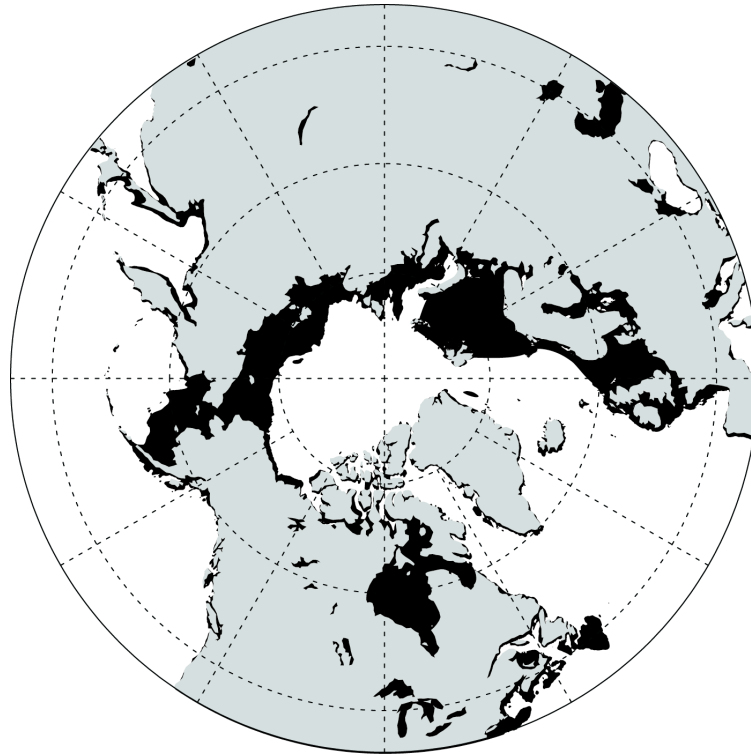

Figure 1: North Polar stereographic map of land and ocean at Last Glacial Maximum and Pre-Industrial. Grey regions are land for both LGM and PI, and "additional" land at LGM, due to lowered sea level, is black .
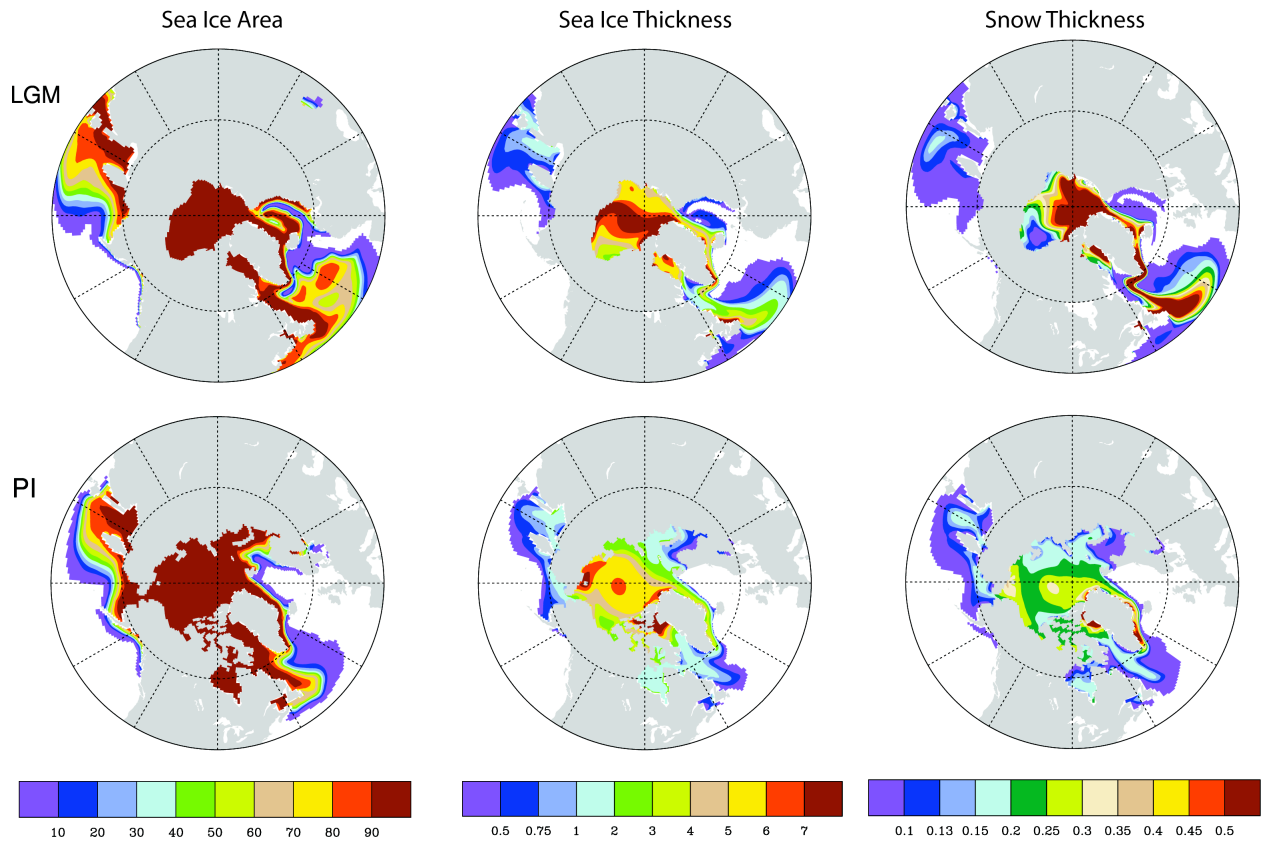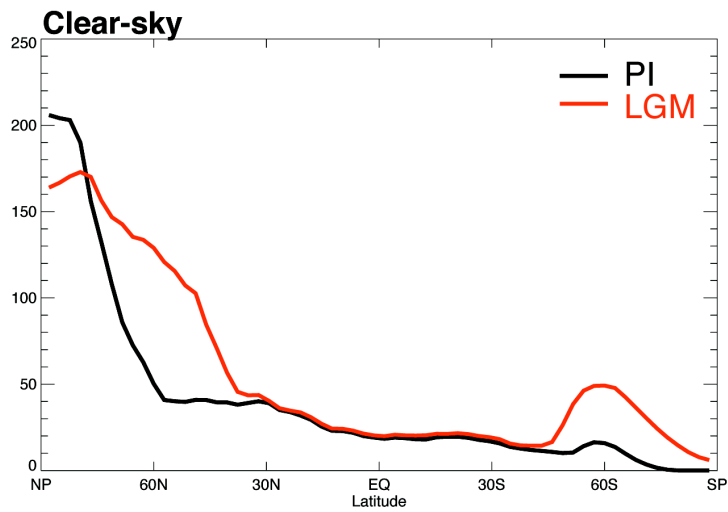
Figure 2: Northern Hemisphere sea ice area in percent (left), sea ice thickness in meters (middle), and snow thickness (right) simulated by the CCSM3 for the LGM (top) and PI (bottom). The month of March was selected because it is the month of maximum sea ice cover in the Northern Hemisphere.

JJA reflected SW at surface

Clear-sky

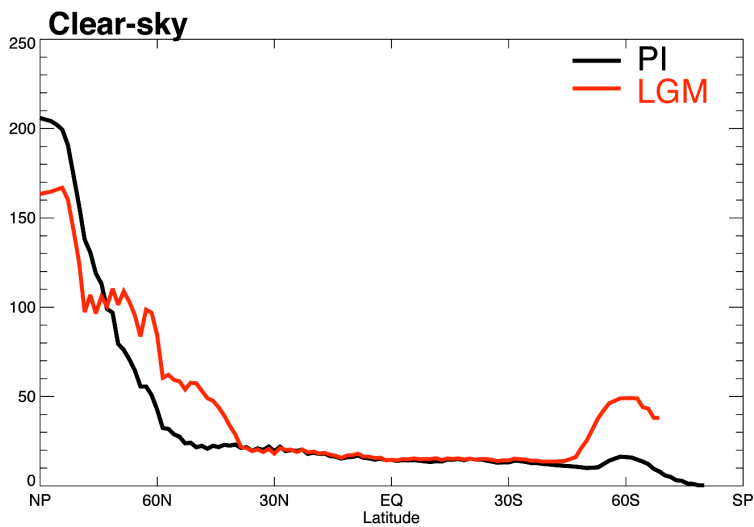**JJA reflected SW at surface (ocean only)**

Clear-sky

Figure 3: June-July-August (JJA) clear-sky and all-sky zonally averaged reflected shortwave radiation in W m^{-2} at the surface for all areas (top) and the ocean only (bottom). Pre-Industrial is shown in black and the Last Glacial Maximum in red.
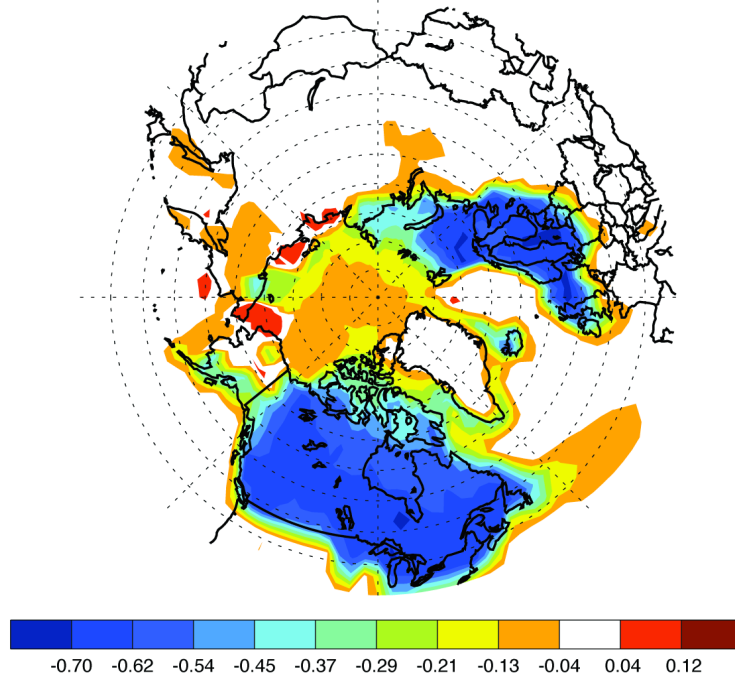
JJA Clear-sky Surface Albedo
W/m2

Figure 4: June-July-August (JJA) clear-sky surface albedo (top) in Wm^{-2} for PI minus LGM. No attempt has been made to reconstruct the continental outlines.